Revista Mexicana de Astronomía y Astrofísica, **47**, 139–158 (2011)

H II REGIONS AND PROTOSOLAR ABUNDANCES IN GALACTIC CHEMICAL EVOLUTION

L. Carigi and M. Peimbert

Instituto de Astronomía, Universidad Nacional Autónoma de México, Mexico

Received 2010 November 18; accepted 2011 February 3

RESUMEN

Presentamos modelos de evolución química del disco galáctico con diferentes rendimientos dependientes de Z. Encontramos que una tasa moderada de pérdida de masa en estrellas masivas de metalicidad solar produce un excelente ajuste con los gradientes de C/H y C/O del disco de la Galaxia. El mejor modelo reproduce: las abundancias de H, He, C y O derivadas de líneas de recombinación en M17, las abundancias protosolares y las relaciones C/O-O/H, C/Fe-Fe/H y O/Fe-Fe/H derivadas de estrellas de la vecindad solar. La concordancia del modelo con las abundancias protosolares implica que el Sol se originó a una distancia galactocéntrica similar a la actual. El modelo para $r = 3$ kpc implica que una fracción de las estrellas en la dirección del bulbo se formó en el disco interno. Nuestro modelo reproduce la relación C/O-O/H derivada de regiones H II extragalácticas en galaxias espirales.

ABSTRACT

We present chemical evolution models of the Galactic disk with different Z-dependent yields. We find that a moderate mass loss rate for massive stars of solar metallicity produces an excellent fit to the observed C/H and C/O gradients of the Galactic disk. The best model also fits: the H, He, C, and O abundances derived from recombination lines of M17, the protosolar abundances, and the C/O-O/H, C/Fe-Fe/H, and O/Fe-Fe/H relations derived from solar vicinity stars. The agreement of the model with the protosolar abundances implies that the Sun originated at a Galactocentric distance similar to the one it has now. Our model for $r = 3$ kpc implies that a fraction of the stars in the direction of the bulge formed in the inner disc. We obtain a good agreement between our model and the C/O versus O/H relationship derived from extragalactic H II regions in spiral galaxies.

Key Words: galaxies: abundances — galaxies: evolution — Galaxy: bulge — H II regions — ISM: abundances — Sun: abundances

1. INTRODUCTION

The comparison of detailed Galactic chemical evolution models, GCE models, with accurate abundance determinations of stars and gaseous nebulae provides a powerful tool to test the chemical evolution models and the accuracy of observational abundance determinations of stars of different ages and of H II regions located at different galactocentric distances.

In this paper we will compare our models with stellar and H II region abundances to test if the H II region abundances derived from recombination lines agree with the stellar abundances, in particular with the protosolar abundances that correspond to those present in the interstellar medium 4.5 Gyr ago. Also, our GCE models can be used to constrain the C yields for massive stars. The C yield is not well known and we will vary it to obtain the best fit between our GCE models and the observational data.

Carigi & Peimbert (2008, hereinafter Paper I) presented chemical evolution models of the Galactic disk for two sets of stellar yields that provided good fits to: (a) the O/H and C/H gradients (slope and absolute value) derived from H II regions based on recombination lines (Esteban et al. 2005) and including the dust contribution (Esteban et al. 1998), and (b) the $\Delta Y/\Delta Z$ value derived from the Galactic H II region M17, and the primordial helium abundance, Y_p obtained from metal-poor extragalactic H II regions (Peimbert, Luridiana, & Peimbert 2007). In Paper I, based on our GCE models and combined with the constraints available, we were not able to discriminate between the stellar evolution models assuming high wind yields for massive stars, HWY, and those assuming low wind yields for massive stars, LWY.

Previous works has focused on the test of stellar yields using GCE models constrained by chemical gradients obtained by different methods, gradients that in general show similar slopes but a considerable spread in the absolute O/H ratios, e.g., Prantzos, Vangioni-Flam, & Chauveau (1994); Carigi (1996); Chiappini, Matteucci, & Meynet (2003a); Romano et al. (2010). To test the stellar yields it is necessary to have good absolute abundance values of stars and H II regions. To determine the O/H abundances of H II regions in irregular and spiral galaxies many methods have been used in the literature. Most of them have been based on fitting photoionized models to observations or on the determination of the electron temperature, T, from the 4363/5007 [O III] ratio directly from observations. A comparison of many of the different methods used has been made by Kewley & Ellison (2008). They find that the O/H differences derived by different methods between two given H II regions amount to 0.10–0.15 dex. On the other hand for all the methods the absolute difference for a given H II region is considerably larger, reaching values of 0.7 dex for extreme cases (see Figure 2 in their paper and the associated discussion). Most of the differences among the various calibrations are due to the temperature distribution inside the nebulae. In this paper we will use only abundances of H II regions based on recombination lines of H, He, C, and O. These lines depend weakly on the electron temperature; they are roughly proportional to $1/T$, therefore the relative abundances among these four elements are practically independent of the electron temperature.

There are two frequently used methods to derive C and O gaseous abundances from H II regions: (a) the most popular one, based on collisionally excited lines (or forbidden lines) and the T(4363/5007) temperatures (the FL method) and (b) the one based on C and O recombination lines (the RL method). The RL method produces gaseous O and C abundances higher by about 0.15 to 0.35 dex than the FL method. The RL method is almost independent of the electron temperature, while the FL method is strongly dependent on the electron temperature. It is possible to increase the FL abundances under the assumption of temperature inhomogeneities to reach agreement with the RL values. The temperature distribution can be characterized by the average temperature, T_0, and the mean square temperature variation, t^2 (e.g., Peimbert 1967; Peimbert, Peimbert, & Luridiana 2002). The t^2 values needed to reach agreement between the RL and the FL abundances are in the 0.02 to 0.05 range, while the photoionization models predict typically t^2 values in the 0.003 to 0.01 range. This discrepancy needs to be sorted out (e.g., Peimbert & Peimbert 2011, and references therein).

Paper I is controversial because the C/H and O/H gaseous abundances of the H II regions have been derived from recombination lines (that is equivalent to the use of $t^2 \neq 0.000$ and forbidden C and O lines) and the assumption that 20% of the O atoms and 25% of the C atoms are trapped in dust grains (0.08 dex and 0.10 dex respectively). These assumptions increase the O/H ratio by about 0.25 to 0.45 dex relative to the gaseous abundances derived from T(4363/5007), the forbidden O and C lines, and the assumption that $t^2 = 0.00$.

Due to the controversial nature of the H II region abundances used in Paper I and noting that we were not able to discriminate between the two sets of stellar yields adopted, we decided to test our GCE models further by including additional observational constrains: (a) the Asplund et al. (2009) protosolar abundances that provide us with the O/H, C/H, Fe/H, and $\Delta Y/\Delta O$ in the interstellar medium 4.5 Gyr ago; (b) the C/H, O/H, and Fe/H by Bensby & Feltzing (2006) for young F and G stars of the solar vicinity; (c) the O/H, C/H, and He/H derived from B stars by Przybilla, Nieva, & Butler (2008); and (d) throughout this paper for all the H II regions we will use abundances derived from recombination lines, and to obtain the total abundances we will increase the gaseous abundances by 0.10 dex in C and 0.12 dex in O to take into account the fraction of atoms trapped in dust grains, except for the metal-poor irregular galaxies for which we will use an 0.10 dex depletion for O (Esteban et al. 1998; Mesa-Delgado et al. 2009; Peimbert & Peimbert 2010).

We also decided to compare our best models with the C/O versus O/H results derived by Esteban et al. (2002, 2009) from bright H II regions in nearby spiral galaxies based on recombination lines, and to make a preliminary discussion of a comparison between our models for $r = 3$ kpc and the stars in the direction of

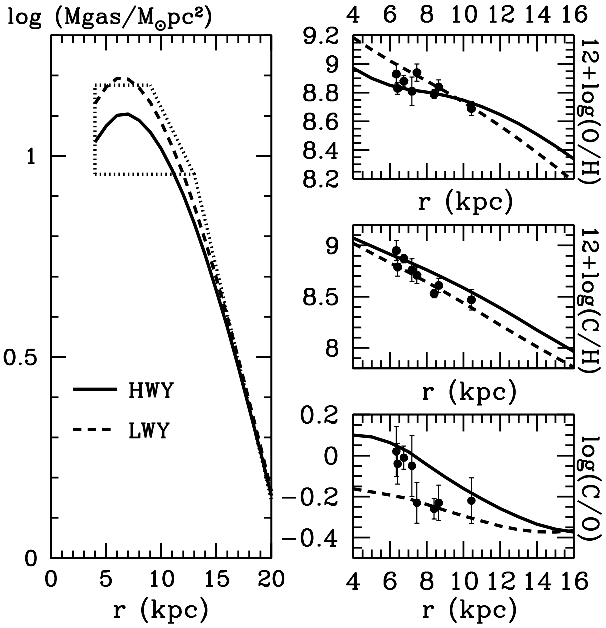

Fig. 1. Present-day radial distribution of: gas surface mass density (left panel), and ISM abundance ratios (right panels). Predictions of our chemical evolution models for the Galactic disk at the present time: HWY (continuous lines), LWY (dashed lines). Observational data: *area enclosed by dotted lines*: average gas surface density distribution by Kalberla & Kerp (2009), *filled circles*: H II regions, gas (García-Rojas & Esteban 2007) plus dust values (see text).

the Galactic bulge obtained by Bensby et al. (2010b) and Zoccali et al. (2008).

The symbols C, O, X, Y, and Z represent carbon, oxygen, hydrogen, helium, and heavy element abundances by unit mass respectively; while C/H, O/H, Fe/H, C/O, C/Fe, and O/Fe represent the abundance ratios by number.

In § 2 we discuss the general properties of the chemical evolution models. We consider infall models for the Galaxy with two sets of stellar yields, the HWY and the LWY. In § 3 we show the prediction of the current abundance gradients for the interstellar medium (ISM) of the Galactic disk and compare them with Galactic H II region abundances derived from recombination lines that include the dust correction. In addition we present for the solar vicinity the chemical history of the ISM and compare it with the chemical abundances of stars of different ages; we define the solar vicinity as a cylinder perpendicular to the Galactic plane, centered on the Sun, with a radius of 0.5 kpc, that extends into the halo to include the stars in the cylinder. In § 4 we compare our chemical evolution models with the protosolar chemical abundances and with those of the H II region M17. Based on the comparison between the observations and the models we present in § 5 a new Galactic chemical evolution model, with intermediate mass loss due to interstellar winds, IWY, that produces considerably better agreement with the observations. In § 6 we compare the IWY model with additional observations, those provided by extragalactic H II regions in spiral galaxies, and those provided by stars in the direction of the Galactic bulge. The conclusions are presented in § 7. A preliminary account of some of the results included in this paper was presented elsewhere (Peimbert et al. 2010).

2. CHEMICAL EVOLUTION MODELS WITH HIGH AND LOW WIND YIELDS

We present chemical evolution models for the Galactic disk. The models have been built to reproduce the present gas mass distribution, (see Figure 1, left panel) and the present-day O/H values for H II regions in the Galaxy for $6 < r(\mathrm{kpc}) < 11$, (see Figure 1, upper right panel) listed by García-Rojas & Esteban (2007). In what follows we describe in detail the characteristics of the models.

(i) In the models the halo and the disk are projected onto a single disk component of negligible width and with azimuthal symmetry; therefore all functions depend only on the galactocentric distance r and on the time t.

(ii) The models focus on $r \geq 4$ kpc; therefore, the physical processes associated with the Galactic bar are not considered.

(iii) The models are based on the standard chemical evolution equations originally written by Tinsley (1980) and widely used to date. See e.g., Pagel (2009), Matteucci (2001), and Prantzos (2008).

(iv) The age of the models is 13 Gyr, the time elapsed since the beginning of the formation of the Galaxy.

(v) The models are built based on an inside-out scenario with infalls that assume primordial abundances $Y_p = 0.2477$, $Z = 0.00$ (Peimbert et al. 2007). The adopted double infall rate is similar to that presented by Chiappini, Matteucci, & Gratton (1997), as a function of r and t, and is given by $\mathrm{IR}(r,t) = A(r)e^{-t/\tau_{\rm halo}} + B(r)e^{-(t-1\mathrm{Gyr})/\tau_{\rm disk}}$, where the halo formed in the first Gyr with a timescale $\tau_{\rm halo} = 0.5$ Gyr, and the disk started forming immediately after with longer timescales that depend on r, $\tau_{\rm disk} = (8\times r/r_\odot - 2)$ Gyr. We adopt 8 kpc for the Galactocentric distance of the solar vicinity, $r_\odot$. The variables $A(r) = 10\ M_\odot\ \mathrm{pc}^{-2} \times e^{-[r(\mathrm{kpc})-r_\odot]/3.5\ \mathrm{kpc}}$

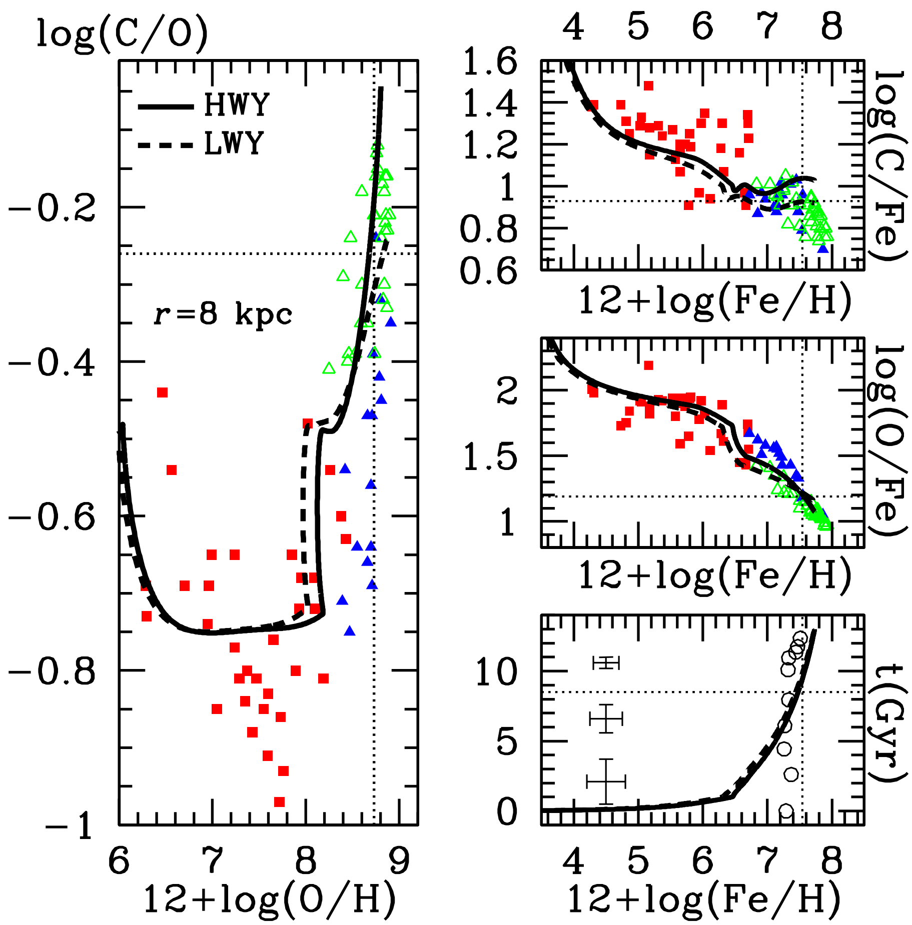

Fig. 2. Chemical evolution models for the solar vicinity (r = 8 kpc): HWY (continuous lines), LWY (dashed lines). The left panel shows the C/O evolution with O/H. The right panels show the evolution of C/Fe and O/Fe with Fe/H, and the Fe/H-time relation. Filled red squares: halo dwarf stars from Akerman et al. (2004). Filled blue and empty green triangles: thick-disk and thin-disk dwarf-stars from Bensby & Feltzing (2006). Dotted lines: protosolar values from Asplund et al. (2009). Open circles: mean ages and Fe/H values of disk stars with better determined ages from Nordström et al. (2004). Horizontal bars: internal dispersions in Fe/H shown by the sample. Vertical bars: age average errors. The color figure can be viewed online.

and $B(r) = 40\ M_\odot\ \mathrm{pc}^{-2} \times e^{-[r(\mathrm{kpc})-r_\odot]/3.5\ \mathrm{kpc}}$ are chosen to match the present-day mass density of the halo and disk components in the solar vicinity, which amount to 0.5 and 49.5 $M_\odot$ pc^{-2}, respectively, where the mass lost by the stars and the halo gas have been incorporated into the disk. Moreover, with the $A(r)$ and $B(r)$ variables the models reproduce the radial profile of the total mass in the Galaxy, $M_{\mathrm{tot}}(r) = 50\ M_\odot\ \mathrm{pc}^{-2} \times e^{-[r(\mathrm{kpc})-r_\odot]/3.5\ \mathrm{kpc}}$ (Fenner & Gibson 2003).

(vi) The models assume the initial mass function (IMF) proposed by Kroupa, Tout, & Gilmore (1993), in the mass range given by 0.08–80.0 $M_\odot$ for $Z > 10^{-5}$, and in the 9.0–80.0 $M_\odot$ mass range for $Z < 10^{-5}$. We consider that Population III does not include objects with less than 9.0 $M_\odot$ and that the change from Pop III to Pop II.5 occurs at $10^{-3.5}Z_\odot$ (Akerman et al. 2004; Bromm & Larson 2004).

(vii) The models include a star formation rate that depends on time and galactocentric distance, $\mathrm{SFR}(r,t) = \nu M_{\mathrm{gas}}^{1.4}(r,t)\ (M_{\mathrm{gas}}+M_{\mathrm{stars}})^{0.4}(r,t)$, taken from Matteucci et al. (1989) and Matteucci & Chiappini (1999), where ν is a constant in time and space. This SFR formula considers the feedback between gas and stars. In our models ν is chosen in order to reproduce the present-day radial distribution of gas surface mass density. We adopted ν values of 0.019 and 0.013 for the HWY and the LWY models, respectively. We assumed a ν value 5 times higher during the halo formation than that adopted for the disk. These ν values combined with the adopted infall rate reproduce the chemical abundances shown by halo and disk stars (see Figure 2).

(viii) The only difference between the HWY and the LWY sets is the assumed mass-loss rate due to stellar winds by massive stars with $Z = 0.02$, see Figure 1 of Carigi & Peimbert (2008). All stellar yields are metal-dependent. We interpolate and extrapolate linearly the yields by mass and metallicity.

The HWY set includes:

(A) For massive stars (MS), those with $8 < m/M_{\odot} < 80$, the yields by: (a) Hirschi (2007) for $Z = 10^{-8}$ (with rotation velocity between 500 and 800 km s^{-1}, depending on stellar mass); (b) Meynet & Maeder (2002) for $Z = 10^{-5}$ and $Z = 0.004$ (with rotation velocity = 300 km s^{-1}); (c) Maeder (1992) for $Z = 0.02$ (high mass-loss rate with no rotation); (d) Since Fe is a chemical element used as observational constraint in most of the chemical evolution models and the Fe yield is not computed by Hirschi (2007), Meynet & Maeder (2002), and Maeder (1992), we adopt Woosley & Weaver (1995) values only for the Fe yields (Models B, for 12 to 30 $M_{\odot}$; Models C, for 35 to 40 $M_{\odot}$; while for $m > 40$ $M_{\odot}$, we extrapolate the $m = 40$ $M_{\odot}$ Fe yields, following Carigi & Hernández 2008). Our models, which include the Fe yields and the O yields by Meynet & Maeder (2002), can reproduce the O/Fe-Fe/H trend of the halo stars (see Figure 2).

(B) For low and intermediate mass stars (LIMS), those with $0.8 \leq m/M_{\odot} \leq 8$, we used the yields by Marigo, Bressan, & Chiosi (1996, 1998) and Portinari, Chiosi, & Bressan (1998) for the $Z = 0.004$ to $Z = 0.02$ range.

(C) For Type Ia SNe we have used the yields by Thielemann, Nomoto, & Hashimoto (1993) in the the SNIa formulation of Greggio & Renzini (1983). A fraction, Abin, of the binary stars of LIMS with a total mass between 3 and 16 $M_{\odot}$ are progenitors of SNIa. We assumed $A\text{bin} = 0.066$ for HWY model, while $A\text{bin} = 0.094$ for LWY models. These fractions are needed to reproduce the age-[Fe/H] relation of the disk stars, the O/Fe-Fe/H relation of the disk stars of the solar vicinity, and the protosolar Fe/H value for each model (see Figure 2).

In the LWY set we have updated the yields of massive stars only for $Z = 0.02$ assuming the yields by Hirschi, Meynet, & Maeder (2005) with rotation velocity = 300 km s^{-1}. The rest of the stellar yields are those included in the high wind set.

(ix) For MS the models include the stellar lifetimes given by Hirschi (2007), Meynet & Maeder (2002), and Hirschi et al. (2005), while for LIMS include the main sequence lifetimes from Schaller et al. (1992).

(x) Due to its deep potential well the models do not consider any type of outflows from the Galaxy. In addition, we disregard outflows of C and O rich material from SNe, because of the small C/O ratios observed in H II regions. See Carigi et al. (1995) and Carigi, Colín, & Peimbert (1999).

(xi) We do not include radial flows of gas or stars.

Since the solar vicinity and the Galactic disk contain stars and H II regions of a broad range of metallicities, our galaxy is a proper laboratory to study the $\Delta Y/\Delta O$ and $\Delta C/\Delta O$ behavior at high Z values and to test observationally the predictions of the HWY and the LWY models. Furthermore, the main elements affected by the winds of massive stars are He, C, and O; therefore, a careful comparison of the abundances predicted by the chemical evolution models with the observed values will allow us to constrain the mass loss rate and consequently the yields of massive stars.

3. THE GALACTIC H II REGION GRADIENTS AND THE CHEMICAL HISTORY OF THE SOLAR VICINITY

In Figure 1 we show the present-day radial distribution of the gaseous mass and the O/H, C/H, and C/O gradients in the Galactic disk predicted by the HWY and LWY models.

For Figure 1 we have chosen observational constraints that represent the current gas mass and the abundances of the Galactic disk. We have taken the average surface density as a function of the Galactic radius derived from H I shown by Kalberla & Kerp (2009) in their Figure 5. We have assumed the abundance ratios of the gas component determined from H II regions based on recombination lines by García-Rojas & Esteban (2007) corrected for dust depletion. It should be noted that the H II regions used by García-Rojas & Esteban (2007) are high density young objects that do not contain WR stars; consequently they have not been polluted by the evolution of their ionizing stars and their O/H and C/H values are representative of the present value of the Galactic interstellar medium.

Based on Figure 1, it can be noted that both models successfully reproduce the current radial distribution of gas surface mass density and the C/H and O/H gradients at the one σ level but neither of them reproduce the C/O gradient for all Galactocentric distances. The HWY model fits the C/O values of H II regions for $r < 7.3$ kpc, while the LWY model does so for $7.5 < r(\text{kpc}) < 9$.

In the literature there are chemical abundance determinations from recombination lines of Galactic H II regions only for $6 < r(\mathrm{kpc}) < 11$. At present, the evidence for the flattening of the Galactic gradients is not conclusive: Vílchez & Esteban (1996) based on H II regions found a flat O/H gradient for $r > 14$ kpc, while more recent work based on Cepheids did not confirm this result, see Mattsson (2010). Additional observations of high quality obtained with the same method are needed to establish the behavior of the gradients for $r > 11$ kpc. With an inside-out scenario without dynamical effects it is difficult to reproduce a possible flattening of the O/H gradient, see Mattsson (2010). Cescutti et al. (2007) in an inside-out scenario reproduce the flattening of radial gradients shown by Cepheids for $r > 7$ kpc assuming a constant surface density for the halo. In our models this is equivalent to adopting a constant $A(r)$, which means that the volumetric density of the halo increases towards the outer parts of the Galaxy, a density distribution that we consider unlikely. According to Roskar et al. (2008) and Sánchez-Blázquez et al. (2009), the flattening is a consequence of stellar migration and of a break in the star formation rate at large radii. A third possibility is that the formation of the Galaxy had a modest stellar formation episode previous to the inside-out scenario. Support for this idea comes from the increase of the average age of the stars at large galactocentric distances (Vlajić, Bland-Hawthorn, & Freeman 2011, and references therein).

In Figure 2 we show the evolution of C/O-O/H, C/Fe-Fe/H, O/Fe-Fe/H, and time-Fe/H relations, predicted by the HWY and LWY models for $r =$ 8 kpc. The time vs Fe/H plot is a representation equivalent to the known age-Z relation of the solar vicinity.

For Figure 2 we have chosen observational constraints that represent the chemical history of the solar vicinity. We have taken dwarf stars of the Galactic halo by Akerman et al. (2004), as representative of the first Gyr of the evolution, and dwarf stars of the Galactic thick and thin disk by Bensby & Feltzing (2006), as representative of the last 12 Gyr of the evolution. Also in Figure 2 we show the mean ages and Fe/H values of disk stars with better determined ages presented by Nordström et al. (2004) in the lower part of their Figure 28. Moreover, we have assumed the protosolar abundances by Asplund et al. (2009) as representative of $t = 8.5$ Gyr.

We converted the chemical abundances determined by Bensby & Feltzing (2006) to abundance ratios by number assuming their own solar abundances, see their paper for references. Also, we normalized the stellar ages by Nordström et al. (2004) to the age of the model (13.0 Gyr).

Based on Figure 2, it can be noted that both models produce a reasonable fit to the C/O-O/H, C/Fe-Fe/H, and O/Fe-Fe/H trends in the solar vicinity. From the C/O-O/H and C/Fe-Fe/H relations it can be seen that the HWY model predicts more C than observed in metal rich disk stars, while the LWY model predicts less than the HWY. Alternatively, both models predict a C/Fe plateau for Fe/H higher than solar, while metal rich stars of the thin disk show a C/Fe decrease. This observed trend could be explained if massive stars of $Z > Z_\odot$ are less efficient in producing C than massive stars of solar metallicity. Stellar yields of MS and LIMS for $Z > Z_\odot$ are needed to obtain a complete picture of the evolution at high Z (Carigi 2008).

Cescutti et al. (2009) and Romano et al. (2010) focused on the C/O-O/H relation shown by thin disk stars of the solar vicinity and found that the C/O rise at high O/H values can be explained partially with metallicity-dependent stellar winds in massive stars (Maeder 1992; Meynet & Maeder 2002). This result is in agreement with our previous conclusions (Carigi 1994, 1996, 2000; Carigi et al. 2005, and Paper I), and with those by Prantzos et al. (1994).

The fit of our models to the time-Fe/H relation shown by disk stars of the solar vicinity is reasonable for $4 < t(\mathrm{Gyr}) < 13$, but our models cannot reproduce the mean behavior of older stars of the Galactic disk. Probably the reason is that some of these stars originated closer to the center of the Galaxy and migrated outwards, or belonged to satellite galaxies with different chemical histories that were captured by our galaxy. Most of the stars of the sample have ages lower than 9 Gyr, corresponding to $t > 4$ Gyr, and the internal dispersion in Fe/H of old disk stars is higher than that of young stars. Both models fit the Fe/H values of the halo stars with ages between 12 and 13 Gyr in the $t < 1$ Gyr range.

The main difference between the HWY and the LWY sets is due to the stellar yields assumed for massive stars at $Z = 0.02$. The HWY assume a relatively high mass-loss rate for massive stars with $Z = 0.02$ (yields by Maeder 1992), while the LWY assume a relatively low mass-loss rate for massive stars with the same Z (yields by Hirschi et al. 2005). Since the mass loss rate is proportional to the stellar metallicity, the efficiency of this rate increases with metallicity and becomes important at $Z \sim Z_\odot$. According to Hirschi et al. (2005) mass loss rates are a key ingredient for the yields of massive stars and the

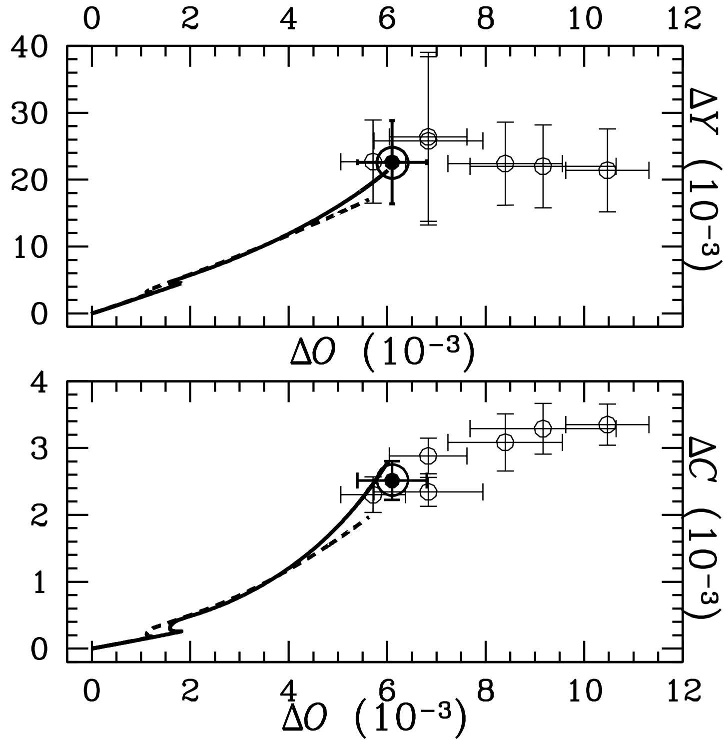

Fig. 3. ΔY vs ΔO (upper panel) and ΔC vs ΔO (lower panel) for the solar vicinity ($r = 8$ kpc). Evolution from $t = 0$ ($\Delta Y = \Delta C = \Delta O = 0$) to 8.5 Gyr (Sun-formation time) predicted by models that assume HWY (continuous lines), and LWY (dashed lines). $\odot$: Protosolar values by Asplund et al. (2009). Open circles: Protosolar values from photospheric data by different authors compiled by Asplund et al. (2009, Table 4) and corrected for gravitational settling (Asplund et al. 2009).

rates assumed by them are 2–3 smaller than those of Maeder (1992). This difference between a high and a low mass-loss rate produces opposite differences in the C and O yields. These differences occur in the pre-SN and in the SN phases. In the pre-SN phase massive stars are able to process He into C, and their stellar winds take away a lot of new C. Since the O production occurs deeper than the C production, the wind contribution to the O yield is much smaller than that to the C yield; consequently C constitutes the largest fraction of heavy elements ejected during the wind phases. While in the SN phase the contribution to the C and O total yields depends mainly on the mass of the CO core, a small fraction of C in the CO core remains unmodified and is ejected during the explosion. Alternatively the O production by the SNe is proportional to an important fraction of the mass of this core; consequently, O constitutes the largest fraction of heavy elements ejected during the SN stage. Therefore, when the initial stellar metallicity is higher, the mass loss rate is higher, the C yield is higher, the CO core is less massive, and consequently the O yield is smaller.

4. THE PROTOSOLAR AND THE PRESENT SOLAR VICINITY ABUNDANCES

To compare GCE models of Y, C, and O with observations we need to use the best abundance determinations available for these elements. We consider that the two most accurate Galactic Y, C, and O determinations are the protosolar values (Asplund et al. 2009) and the M17 H II region values (Paper I).

4.1. *Protosolar abundances*

In order to study the time-agreement with the protosolar values, we show in Figure 3 the predicted evolution of ΔY vs ΔO and ΔC vs ΔO from 0 to 8.5 Gyr (the Sun-formation time). The ΔY value for Figure 3 (and throughout this paper) is given by $\Delta Y = Y - Y_p$, where Y_p is the primordial He abundance, which amounts to 0.2477 (Peimbert et al. 2007). In this figure $\Delta O = O$, and $\Delta C = C$ because at the time of the primordial nucleosynthesis O and C are not produced. For $t = 0$ the models start at ΔY, ΔO, and ΔC equal to zero, and in this figure the evolution of the models stops at $t = 8.5$ Gyr, the time the Sun was formed. Also, in this figure we present some of the most popular Y, C, and O protosolar abundances published in the last 21 years. These photospheric solar abundances were obtained by Anders & Grevesse (1989), Grevesse & Noels (1993), Grevesse & Sauval (1998), Lodders (2003), Asplund, Grevesse, & Sauval (2005), and Lodders, Palme, & Gail (2009); these abundances were compiled by Asplund et al. (2009) in their Table 4. To obtain the protosolar abundances of the heavy elements, the photospheric abundances were increased by 0.04 dex, which takes into account the effect of gravitational settling. We used the protosolar X values shown in Table 4 by Asplund et al. (2009) to change the abundances by number to abundances by mass.

From Figure 3 it can be noted that: (a) the HWY model fits very well the Y and O protosolar values, while the predicted C is about 1σ higher than observed. (b) The LWY model matches the Y and O protosolar values within 1σ, but the predicted C is about 2σ lower than observed. (c) The solar abundances predicted by our models are in much better agreement with the recent He, C, and O protosolar values determined by Asplund et al. (2009) than with the previous ones compiled by them. (d) The He protosolar abundance determinations have remained almost constant over the years, while the C and O ones have decreased.

4.2. ΔY *vs* ΔO *evolution compared with M17 and young B stars of the solar vicinity*

In Figure 4 we present the evolution of ΔY versus ΔO. The models presented in this figure for r equal to 6.75, 8, and 17 kpc correspond to the 0 to 13 Gyr range. The data should be compared with the end point of the evolution of the corresponding evolutionary track. In Figures 4, 5 and 7 the evolutionary tracks and the related observational data have the same color.

Since there are no good abundance determinations for the outer parts of the Galactic disk, we test our models with data of irregular galaxies. Therefore, in Figure 4 we show the ΔY and ΔO values of the metal poor extragalactic H II regions determined by Peimbert et al. (2007). Specifically, we compare our 17 kpc track with NGC 2366, because it contains one of the brightest H II regions of nearby galaxies. The gaseous O abundances of the metal poor H II regions were increased by 0.10 dex to include the fraction of O atoms embedded in dust grains inside the H II regions (Peimbert & Peimbert 2010). From that figure it can be noticed that the predicted chemical evolution of the Galaxy for large Galactocentric radii ($r > 17$ kpc) at $t = 13$ Gyr behaves like that of irregular galaxies at the present time.

In Figure 4 we also present the abundances of B stars of the solar vicinity derived by Przybilla et al. (2008). We have adopted the Orion X value shown in Carigi, Colín, & Peimbert (2006) for converting Xi/H (the abundance ratio by number of any i element) of B stars to Xi by mass. The ΔY abundance derived from B stars is in good agreement with the HWY and LWY models for $r = 8$ kpc. On the other hand, the ΔO value is about 1.5σ and about 4.5σ smaller than the values predicted by the HWY and LWY models, respectively. The O/H values derived by Simón-Díaz (2010) for the B stars of the Orion star forming region are in good agreement with the Przybilla et al. (2008) determinations.

We decided to include as observational constraints the O and He abundances of the H II region M17. This object has the best He abundance determination available because its degree of ionization is very high and the correction for neutral helium, which is always indirect, is the smallest one of the well observed Galactic H II regions (see Paper I). We show in Figure 4 two sets of ΔO values, one derived from O recombination lines, and the other derived from the O forbidden lines under the assumption that $t^2 = 0.00$.

The point with the highest ΔY and ΔO values of the HWY model at 6.75 kpc presented in Figure 4 (the point at $t = 13$ Gyr) should be compared with the two M17 values. The ΔY model value is in good agreement with the two M17 values. The ΔO value for $t^2 = 0.00$ is more than 5σ smaller than the model prediction, while the $t^2 \neq 0.00$ point is less than 2σ higher than the ΔO model prediction. For the LWY model the predicted ΔY value is in good agreement with the two M17 values; but the ΔO value of the $t^2 = 0.00$ point is 12σ smaller than the model prediction, while the ΔO value of the $t^2 \neq 0.00$ point is less than 2σ smaller than the model prediction. Based on this comparison we conclude that it is possible to get an excellent agreement with the $t^2 \neq 0.00$ ΔO value using a model with yields intermediate between the HWY and the LWY models, but that it is not possible to find a reasonable model to fit the ΔO value derived assuming $t^2 = 0.00$.

Since the HWY and the LWY models fit the protosolar values and produce a reasonable fit to the observed M17 ΔO and ΔY values, we conclude that the protosolar values in the context of Galactic chemical evolution provide a strong consistency check to the O recombination abundances derived from H II regions, and are in disagreement with the O abun-

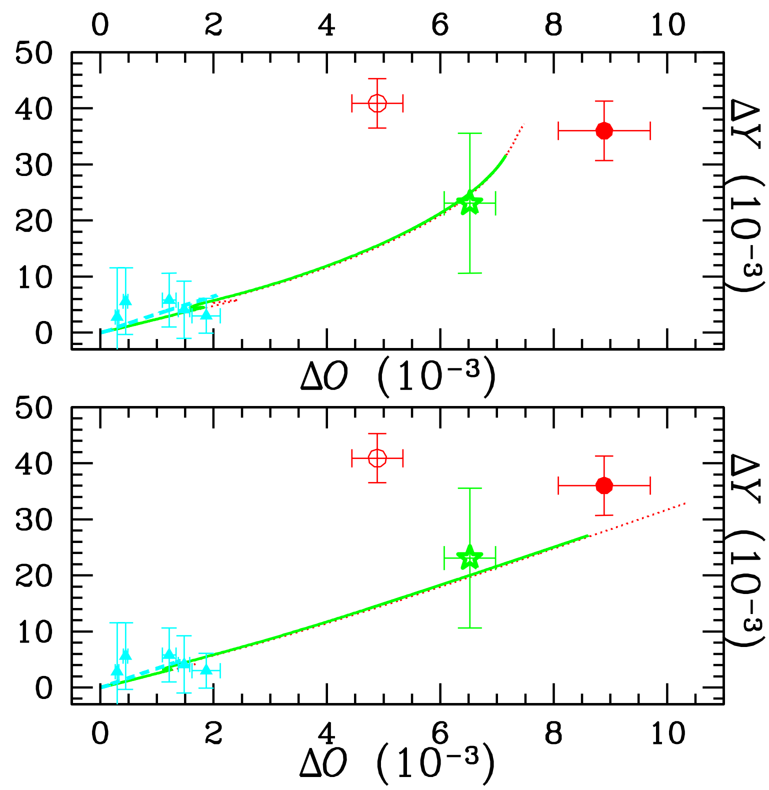

Fig. 4. Evolution of ΔY vs ΔO. The HWY model is shown in the upper panel and the LWY model in the lower panel. Chemical evolution tracks from 0 ($\Delta Y = \Delta O = 0$) to 13 Gyr (present time) for r = 6.75, 8, and 17 kpc (dotted-red, solid-green, and dashed-cyan lines, respectively). The three tracks in each panel partially overlap, from top to back they lie as follows: 17 kpc, 8 kpc, and 6.75 kpc. The values for the H II regions and the B stars correspond to 13 Gyr. The M17 H II region at r = 6.75 kpc is represented by a filled circle for t^2 = 0.036 (RL) and by an open circle for t^2 = 0.00 (FL). The solar vicinity B stars value by Przybilla et al. (2008) is represented by a star. The extragalactic low metallicity H II regions are represented by filled triangles for $t^2 \neq 0.00$ (FL) (Peimbert et al. 2007). A $Y_p = 0.2477$ is adopted (Peimbert et al. 2007). The color figure can be viewed online.

dances derived from forbidden lines under the assumption that t^2 = 0.00. Additional support for this result is provided by Simón-Díaz & Stasińska (2011) who, based on a study of 13 B-type stars of the Orion star forming region OB1, find that the stellar O/H abundances agree much better with the Orion H II region abundance derived from recombination lines than with that derived from collisionally excited lines.

4.3. *ΔC vs ΔO evolution compared with H II regions, and young B, F, and G stars of the solar vicinity*

In what follows we will discuss the ΔC and ΔO observational values adopted from the literature and we will compare them with the HWY and LWY model predictions. In Figure 5 we show the 0–13 Gyr evolution of the ΔC-ΔO relation for r = 7, 8, and 17 kpc.

The O/H ratio of the LWY model for r = 17 kpc and t = 13 Gyr corresponds to the O/H value of NGC 2363, the extragalactic metal-poor H II region best suited for our purpose. This model is in good agreement with the C/O observed ratio. Similarly the O/H ratio of the HWY model for r = 17 kpc and t = 13 Gyr corresponds to the O/H value of NGC 2363. This model is also in good agreement with the C/O observed ratio. The ΔO gas and dust values for NGC 2363 are those presented in Figure 4, while the ΔC value includes gas (Esteban et al. 2009) and dust components. We have considered the Y and O/Z values from Peimbert et al. (2007) to calculate X for NGC 2363 and to change the abundances by number to abundances by mass.

For $r \sim 8$ kpc and t = 13 Gyr there are several reliable C and O abundance determinations for the solar vicinity. To compare our models with observations we chose: (a) the average C/H and O/H values

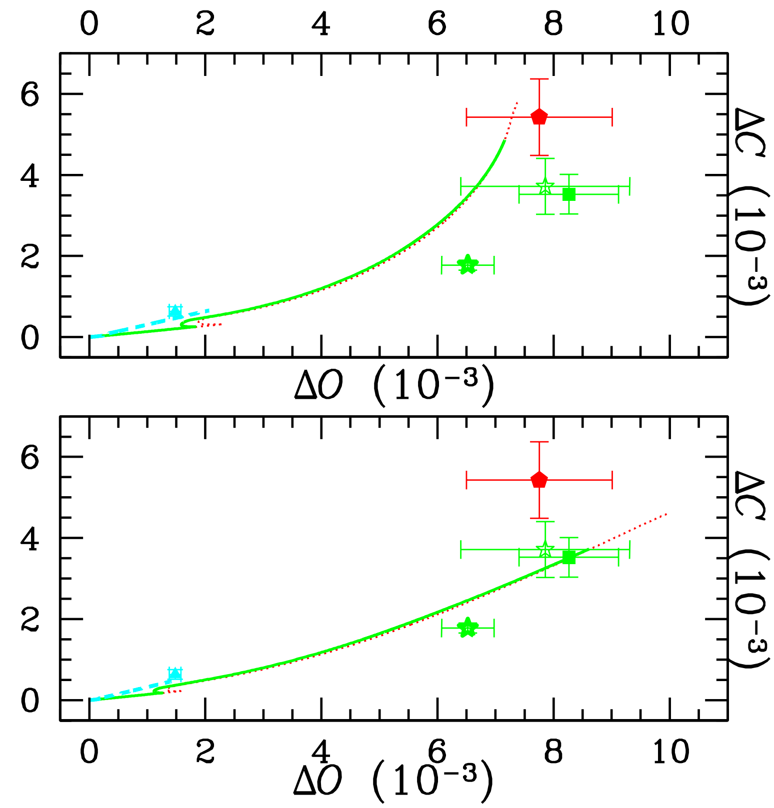

Fig. 5. ΔC vs ΔO diagram. The dotted red line represents the chemical evolution track from 0 ($\Delta C = \Delta O = 0$) to 13 Gyr (present time) for $r = 7$ kpc, the other lines as in Figure 4. A description of the symbols follows. Filled pentagon: Average values of the M17 and M20 H II regions at $r = 6.75$ and 7.19 kpc, respectively. Empty star: Average values of young F-G dwarf stars of the solar vicinity, $r \sim 8$ kpc, from Bensby & Feltzing (2006) (see text). Filled square: Average values of NGC 3576 and Orion H II regions at $r = 7.46$ and 8.40 kpc. Filled star: Average value of B stars by Przybilla et al. (2008). Filled triangle: NGC 2363 H II region in a very metal-poor irregular galaxy (see text). The color figure can be viewed online.

of NGC 3576 and Orion H II regions at $r = 7.46$ and 8.40 kpc, and the correction for the fractions of C and O embedded in dust grains; (b) the young F and G dwarf stars studied by Bensby & Feltzing (2006); (c) the average C and O values of B stars by Przybilla et al. (2008).

In Figure 5 we compare our models with the average ΔC and ΔO values of NGC 3576 and Orion, and find a reasonable agreement. To convert the Xi/H values by number to Xi by mass we adopted the X(Orion) value shown by Carigi et al. (2006).

Bensby & Feltzing (2006) studied 51 F and G dwarf stars of the solar vicinity, 35 belonging to the thin disk and 16 to the thick disk. To compare the abundances predicted by our models with those of the youngest stars presumably recently formed, it is necessary to select the youngest subset of the thin disk stars. The metal richest stars are expected to be the youngest ones. We made three subsets of the metal richest stars of the thin disk containing 4, 8, and 16 objects respectively, and obtained 12+log(O/H) average values of 8.87, 8.84, and 8.83 respectively, and 12+log(C/H) average values of 8.63, 8.64, and 8.59 respectively. In Figure 5 we present the subset of 8 stars as representative of the present day ISM, where we have adopted the X(Orion) by mass (Carigi et al. 2006) for converting Xi/H to Xi by mass. The agreement is very good. As we saw above, the other two subsets of F and G stars produce similar C/H and O/H values, also in good agreement with our models.

To convert the C and O abundances by number to abundances by mass of the B stars by Przybilla et al. (2008) we have taken the Orion X value shown in Carigi et al. (2006). From Figure 5 it can be seen that the ΔC value derived for the B stars is many sigma smaller than that predicted by the HWY and the LWY models. Moreover, it is also considerably

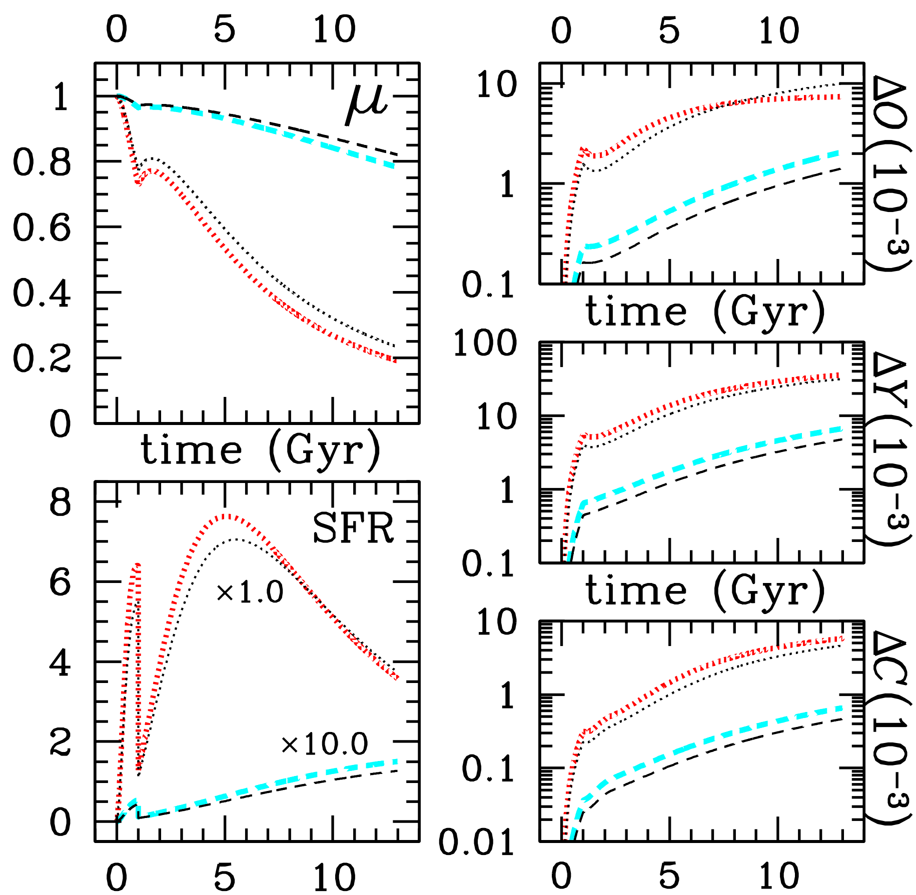

Fig. 6. Evolution of $M_{\rm gas}/M_{\rm tot} = \mu$, star formation rate, ΔO, ΔY, and ΔC for $r = 7$ kpc (dotted lines) and $r = 17$ kpc (dashed lines), assuming HWY (thick tracks) or LWY (thin tracks). Star formation history is in $M_\odot$ pc^{-2} Gyr^{-1} units and the SFR for $r = 17$ kpc has been multiplied by 10.

smaller then the values derived from the F-G dwarf stars and the average of NGC 3576 and the Orion nebula. Maybe part of the reason for the smaller C abundance in the B stars can be due to rotational mixing (e.g., Meynet & Maeder 2000; Fierro & Georgiev 2008). The B stars ΔO value is about 1.5σ and about 4.5σ smaller than the predicted HWY and LWY model values, respectively. Furthermore, the B stars ΔO value is in fair agreement with the F-G dwarf value and about 1.5σ smaller than the the average value of NGC 3576 and Orion. These differences between the B stars and the other objects of the solar vicinity should be studied further.

For $r = 7$ kpc and $t = 13$ Gyr we took the average of the abundances of the M17 and M20 H II regions as the observational constraint; the C/H and O/H gaseous values were obtained from García-Rojas & Esteban (2007) and Paper I, using recombination lines of C and O. We have adopted the M17 X value obtained in Paper I to convert the abundances by number of M17 and M20 to abundances by mass. Unfortunately, there are no observational data representative of the chemical past at $r = 7$ kpc.

The HWY model fits very well the current C and O values for $r = 7$ kpc and marginally the present-day O for $r = 8$ kpc, but does not explain the current C value for $r = 8$ kpc. Alternatively the LWY model fits quite well both the C and O values for the solar vicinity, but predicts a higher O abundance for $r =$ 7 kpc.

In Figures 4 and 5 the evolutionary tracks partially overlap: for a given ΔO value the ΔY and ΔC values of the two different tracks are almost the same, but the time is very different. In Figure 6 we present the evolution of ΔO, ΔY, and ΔC as a function of time to appreciate the differences between the 7 kpc and the 17 kpc tracks. It is important to present the behavior of $\mu = M_{\rm gas}/M_{\rm tot}$ because it drives the O evolution. For example, the 17 kpc track reaches a ΔO value of about 2×10^{-3}

at 13 Gyr, while the 7 kpc track reaches this value at less than 1 Gyr, whereas the same ΔO value for both tracks occurs at a similar μ value. The small differences in ΔO, ΔY, and ΔC at a given μ value come from: (a) the delay in the C and He enrichment of the ISM due to LIMS, (b) the shape of the SFR, and (c) the differences between the HWY and LWY. In Figure 6 we also present the SFR behavior. It can be seen that for $r = 7$ kpc the SFR is not only different in shape to the one at $r = 17$ kpc but it is from one to two orders of magnitude higher.

From the HWY model it has been found that about half of ΔY and ΔC have been formed by LIMS and half by MS, (see Figure 3 of Carigi et al. 2005, and Figure 6 of Paper I), while most of the ΔO has been formed by MS. LIMS produce a very small amount of O according to yields by different authors (see Figure 7 of Karakas & Lattanzio 2007). In this paper we are using the yields by Marigo and collaborators (1996, 1998). For the LWY model the fractions of ΔY and ΔC due to MS are similar but smaller than for the HWY model. The similar fraction of C and He produced by MS and LIMS is also responsible for the behavior in Figures 4 and 5, where it can be seen that the $\Delta Y/\Delta O$ and the $\Delta C/\Delta O$ relations are similar for the HWY model and for the LWY model for $\Delta O < 5 \times 10^{-3}$.

5. INTERMEDIATE WIND YIELDS

From Figures 1–5 we conclude that the HWY and LWY models are in very good agreement with some of the data, but for other data the agreement is only fair. To improve the agreement with the observations, we suggest the use of intermediate wind yields (IWY) for the computation of the chemical evolution models. We define the IWY as the average of HWY and LWY.

In Figure 7 we present the chemical abundance predictions derived from the IWY model for the most critical observations. In particular, we stress the remarkable fit of the model with the observed values for: (a) the present-day ($t = 13$ Gyr) C/O gradient in the $6 < r(\text{kpc}) < 11$ range with the gradient derived from Galactic H II regions; (b) the $t = 13$ Gyr and $r = 7$ kpc ΔY, and ΔO values with those of M17; (c) the $t = 13$ Gyr and $r = 7$ kpc ΔC, and ΔO values with the average of the M17 and M20 values; (d) the $t = 13$ Gyr and $r = 8$ kpc ΔC, and ΔO values with the average values for NGC 3576, and Orion, and for young F and G stars of the solar vicinity; (e) the $t = 8.5$ Gyr and $r = 8$ kpc ΔY, ΔC, and ΔO values with the protosolar values.

The fits presented in Figure 7 imply that the effects of migration have not been very important in the chemical history of the Galaxy. A similar conclusion on the migration effects for the solar vicinity has been found by Navarro et al. (2011) based on the kinematic properties and the metallicity of thin disk stars.

6. POSSIBLE IMPLICATIONS FOR OTHER SYSTEMS

In is important to study how general is the chemical evolution model derived for the disk of the Galaxy, and to explore its relationship with other spiral galaxies and the transition region between the disk and the bulge of the Galaxy. In what follows we present a preliminary discussion of these two topics.

6.1. *Other spiral galaxies*

Since the IWY model successfully reproduces the He, C, and O abundances in the Galactic disk and in the solar vicinity, we want to extend our study to other spiral galaxies with abundances determined by recombination lines in H II regions.

In Table 1 we collect the gaseous abundances of eight extragalactic H II regions belonging to four spiral galaxies: M31, M33, M101, and NGC 2403 (Esteban et al. 2002, 2009). We have included dust corrections identical to those considered for Galactic H II regions. Consequently, these data are consistent with the Galactic data used in our previous figures (e.g., Figure 7). In Table 1 we show the name and type of the host galaxy, and the name and the galactocentric distance of each extragalactic H II region.

In Figure 8 we show the present-day C/O and O/H values for $r = 4, 5, ..., 15, 16$ kpc (from right to left) predicted by the IWY model of the Galactic disk and the extragalactic H II regions values shown in Table 1.

We notice that in the C/O-O/H relation presented in Figure 8: (a) the spiral galaxy disks have a behavior similar to that of the Milky Way disk; (b) all the extragalactic H II regions of the sample are well reproduced by IWY models; and (c) we see the effect of the Z dependent yields for 12+log(O/H) > 8.4. More determinations of the O/H and C/H ratios in extragalactic H II regions with 12+log(O/H) values < 8.4 and > 8.8 are needed to further test the yields.

Since the general C/O-O/H trend of the extragalactic H II regions can be addressed using the results of the GCE model, we suggest that the four extragalactic spiral galaxies have a similar IMF, no selective outflows, and probably an inside-out formation scenario like our galaxy.

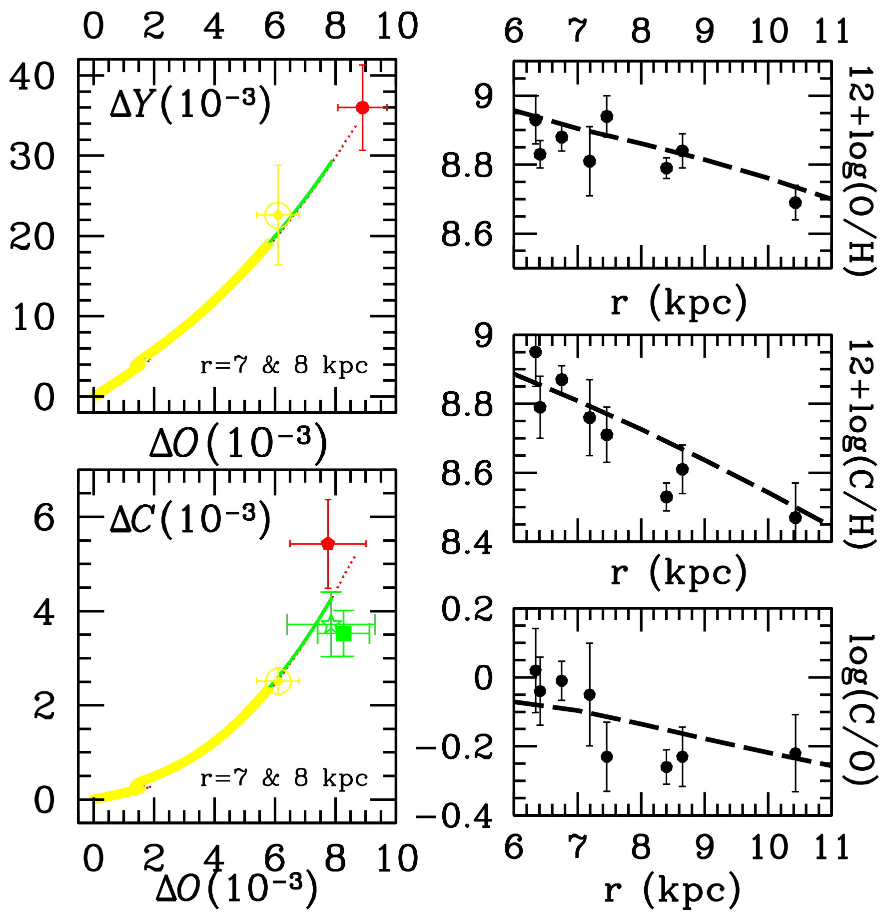

Fig. 7. Chemical evolution model assuming IWY=(HWY+LWY)/2.0. The left panels show the 0–13 Gyr evolution of ΔY vs ΔO and of ΔC vs ΔO for $r = 7$ kpc (dotted red lines) and $r = 8$ kpc (thin solid green line), data as in Figures 4 and 5; the thick yellow lines show the evolution from 0 to 8.5 Gyr for $r = 8$ kpc, data as in Figure 3. The right panels show the present-day ISM abundance ratios as a function of Galactocentric distance, data as in Figure 1. The color figure can be viewed online.

TABLE 1

EXTRAGALACTIC H II REGIONS

Host Galaxy	Type of Galaxy	Object	r (kpc)	12+log(O/H)[a]	12+log(C/H)[a]	log(C/O)[a]
M 101	ScdI	H1013	5.50	8.85 ± 0.09	8.67 ± 0.12	−0.08± 0.15
		NGC 5461	9.84	8.61 ± 0.06	8.30 ± 0.20	−0.21± 0.22
		NGC 5447	16.21	8.64 ± 0.06	8.20 ± 0.12	−0.34± 0.14
		NGC 5471	23.45	8.35 ± 0.15	7.79 ± 0.19	−0.46± 0.24
M 33	ScdII-III	NGC 595	2.87	8.81 ± 0.05	8.63 ± 0.12	−0.18± 0.13
		NGC 604	4.11	8.72 ± 0.03	8.40 ± 0.11	−0.22± 0.12
M 31	SbI-II	K932	16.0	8.74 ± 0.03	8.49 ± 0.13	−0.18± 0.14
NGC 2403	ScdIII	VS44	2.77	8.73 ± 0.04	8.32 ± 0.18	−0.31± 0.19

[a]Gaseous value plus dust correction.

TABLE 2

ABUNDANCE GRADIENTS NORMALIZED TO R_0[a]

Galaxy	R_0(kpc)[b]	12+log(O/H)	12+log(C/H)	log(C/O)
M101	28.95	$-0.492 \times (r/R_0)+8.84$	$-1.32 \times (r/R_0)+8.99$	$-0.65 \times (r/R_0)+0.03$
M33	6.83	$-0.492 \times (r/R_0)+9.00$	$-0.72 \times (r/R_0)+8.93$	$-0.22 \times (r/R_0)-0.10$
MW	11.25	$-0.495 \times (r/R_0)+9.16$	$-1.16 \times (r/R_0)+9.50$	$-0.65 \times (r/R_0)+0.34$

[a] R_0 = galactic photometric radius to 25 mag per square second.

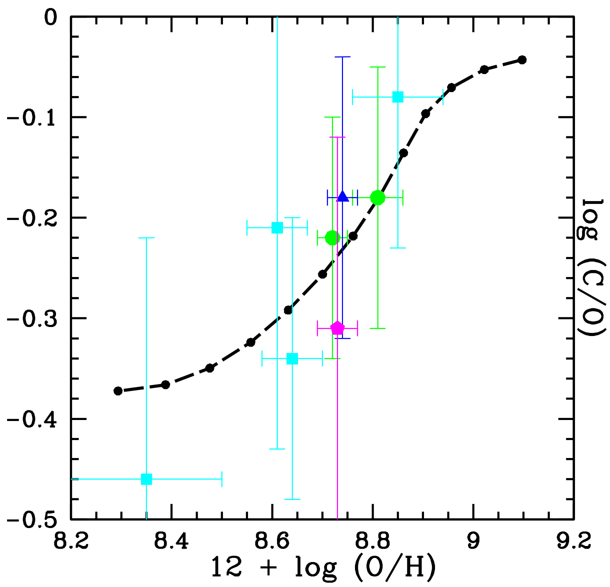

Fig. 8. C/O-O/H values at 13 Gyr predicted by IWY model (long-dashed lines). Small black circles: model predictions at different Galactocentric distances, from 4 kpc (right) to 16 kpc (left). Observed abundances ratios of extragalactic H II regions in spiral galaxies: cyan squares: M101, big green circles: M33, blue triangle: M31, and magenta pentagon: NGC 2403. The color figure can be viewed online.

It should be clear that Figure 8 does not correspond to models of the four spiral galaxies, and that the r values correspond to our galaxy and not to the other galaxies.

In Table 2 we present some galactic information for M33, M101, and the Milky Way, the only galaxies with determinations of chemical gradients based on recombination lines. Specifically, we show the galactic photometric radius to 25 mag per square second (R_0) and the chemical gradients normalized to R_0 corrected for dust depletion (Esteban et al. 2002, 2005, 2009). The MW R_0 was taken from de Vaucouleurs & Pence (1978).

In Figure 9 we show the O/H, C/O, and C/O values as a function of r normalized to R_0 for the eight extragalactic and the eight Galactic H II regions presented in Figures 8 and 7, respectively. Moreover we display the chemical gradients shown in Table 2.

From Figure 9, it can be noted that: (i) the O/H slope for the three galaxies is the same within the errors, which suggests that for a given galaxy the O/H gradient normalized to R_0 is a more meaningful representation than the standard gradient; (ii) the O/H gradients extend from $r/R_0 \sim 0.2$ to $r/R_0 \sim 1.0$; (iii) the O/H ratio at a given r/R_0 differs by a constant among M33, M101 and the MW; and (iv) for 12+log(O/H)$\sim$8.8 the slopes of the C/H and C/O gradients become steeper.

The parallel behavior of the O/H gradients when they are plotted relative to r/R_0 is remarkable, suggesting that the main mechanisms involved in the formation and evolution of spiral galaxies are similar.

The slope of the O/H gradients is similar, but the O/H absolute value at a given r/R_0 is different for each galaxy. In particular the MW shows an O/H ratio 0.24 dex higher than the average of M33 and M101 at a given r/R_0. Considering that the MW is an Sbc galaxy and M33 and M101 are Scd galaxies, this result probably implies that the earlier the type of a galaxy the higher the O/H value at a given r/R_0. This result might be due to the fact that the earlier the bulk of star formation occurs, the fainter the stellar luminosity at a given O/H value and consequently the higher the O/H value at a given R_0 value. More high accuracy determinations of O gradients in spiral galaxies are needed to test this result.

From Figures 8 and 9 it follows that we need: (i) to increase the r/R_0 coverage, mainly for smaller galactocentric distances, with abundance determinations of high accuracy; (ii) to increase the sample by including spiral galaxies of different types; and (iii) to make specific models for each galaxy. All this is

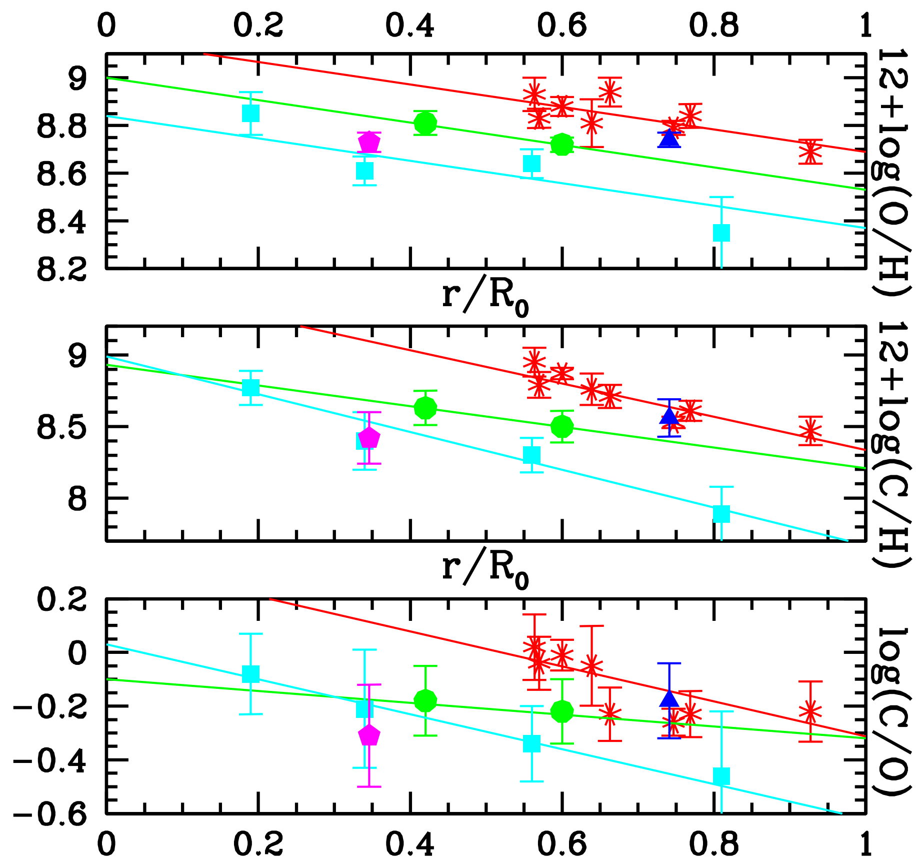

Fig. 9. Chemical abundance ratios of H II regions normalized to galactic photometric radius (R_0) for each galaxy (see Tables 1 and 2). Milky Way: red asterisks (see Figure 7). Others spiral galaxies: symbols as Figure 8. Lines represent the Galactic disk gradients of M101, M33, and the Milky Way. The color figure can be viewed online.

necessary in order to sort out possible differences in the galactic formation and evolution relative to that of the Galaxy and to understand the peculiar behavior of metal-rich stars and H II regions, see Carigi (2008), as well as to test stellar yields for $Z > Z_\odot$.

The present paper only includes specific models for our galaxy. We now present a preliminary discussion on the probable relevance of our results to the study of other spiral galaxies. It is beyond the scope of this paper to produce models for other galaxies and therefore to present a detailed comparison with the results derived by other authors, e.g., Chiappini, Romano, & Matteucci (2003b); Mollá & Díaz (2005); Renda et al. (2005); Yin et al. (2009); Marcon-Uchida, Matteucci, & Costa (2010); Magrini et al. (2010), using different sets of data. In future papers we plan to present detailed models for M31 (Meneses-Goytia, Carigi, & García-Rojas 2011) and M33 (Robles-Valdez, Carigi, & Bruzual 2011, in preparation).

6.2. *The transition region between the inner disk and the Galactic bulge*

A fraction of the stars observed in the direction of the Galactic center might have been formed in the true bulge and another fraction in the inner Galactic disk. Therefore we considered interesting to compare our IWY model for the innermost part of the disc with the abundances for these stars.

Since the inside-out model adopted as the Galactic formation scenario in this paper diverges for $r =$ 2 kpc (see § 2), we obtained the chemical evolution of the innermost ring of the Galactic disk that our GCE model is able to consider, $r = 3 \pm 0.5$ kpc (with a 1 kpc width). The Galaxy at this radius formed efficiently: during the first Gyr the halo formed with a collapse time-scale of 0.5 Gyr and then the disk formed with a formation time scale of 1.0 Gyr. At the end of the evolution (t = 13 Gyr) the gaseous mass amounts to 7% of the baryonic mass inside the $r = 3 \pm 0.5$ kpc ring.

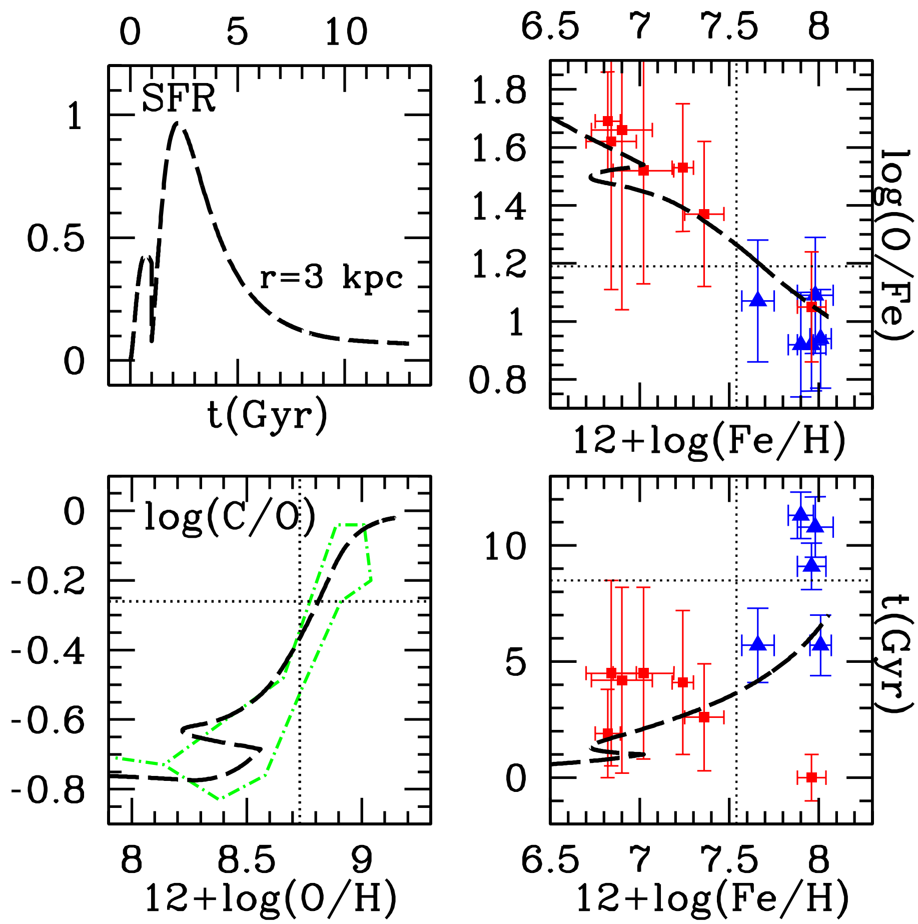

Fig. 10. Evolution for $r = 3$ kpc predicted by the IWY model (long-dashed black lines). Star formation history normalized to 70 $M_{\odot}$ pc^{-2} Gyr^{-1}. C/O-O/H, O/Fe-Fe/H, and time-Fe/H relations from 0 to 7 Gyr. Area enclosed by dot-short-dashed-green lines: Galactic bulge red giant stars presented by Cescutti et al. (2009). Filled symbols: microlensed dwarf and subgiant stars in the Galactic bulge from Bensby et al. (2010b), red squares: old stars with mean age of 9.8 ± 4.0 Gyr, blue triangles: young stars with mean age of 4.5 ± 1.6 Gyr. Ages were normalized to the age of the models (13 Gyr.) Dotted lines: protosolar values from Asplund et al. (2009). The color figure can be viewed online.

In Figure 10 we show the C/O-O/H, O/Fe-Fe/H, and Fe/H evolution obtained with the IWY model between 0 and 7 Gyr. We include the evolution from 0 to 7 Gyr and exclude the 7–13 Gyr range because at 7 Gyr the model reaches the highest Fe/H value shown by the stellar data. Moreover, in the excluded range the SFR is very low and the probability of forming stars younger than 6 Gyr (in the 7 to 13 Gyr range) is negligible.

In Figure 10 (C/O-O/H panel) we show also the area covered by the data of Cescutti et al. (2009). These authors collected [C/O] and [O/H] ratios for the Galactic bulge red giants determined by Fulbright, McWilliam, & Rich (2007) and Meléndez et al. (2008), and used the observed data to obtain the initial stellar C/H and O/H values relative to the solar abundances due to Asplund et al. (2005). In order to convert the Cescutti et al. (2009) data to abundances by number we used, only in this figure, the solar abundances by Asplund et al. (2005). For the other figures, we assumed the protosolar abundances by Asplund et al. (2009).

A description of the model in the C/O-O/H panel of Figure 10 follows. During the halo formation, the IWY model predicts an increase of 12+log(O/H) to 8.6 dex and an increase of 12+log(C/O) to -0.7 dex. After the halo formation finishes, at $t = 1$ Gyr, the O/H ratio decreases due to the dilution produced by the enormous amount of primordial gas that is accreted to form the disk. Later on, this accretion causes a rapid SFR increase, producing an O/H increase. The C/O rise from -0.7 dex to -0.5 dex

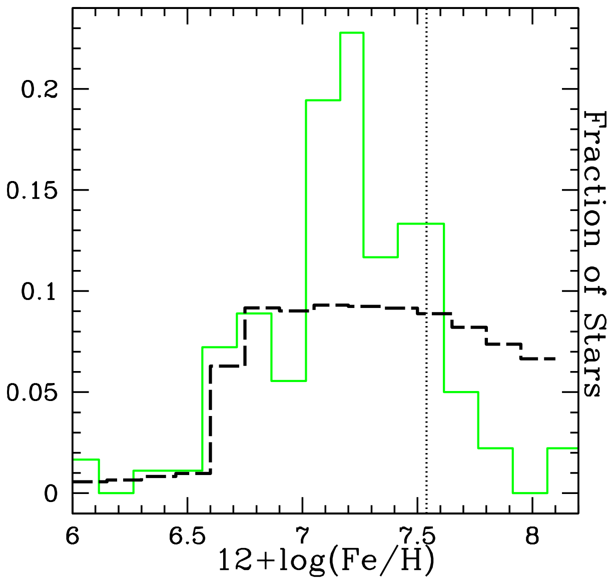

Fig. 11. Iron distribution function. Predictions for $r = 3$ kpc model that assume IWY (long-dashed black line) until 7 Gyr. Observed distribution for the outermost fields ($b = -12$) along the bulge minor axis by Zoccali et al. (2008) (continuous green line). Dotted line: protosolar Fe/H value from Asplund et al. (2009). The color figure can be viewed online.

is due mainly to LIMS, while the C/O rise from -0.5 dex to 0.0 dex is due to both massive stars and LIMS.

In Figure 10 (O/Fe-Fe/H and time-Fe/H panels), we included the chemical abundances determined by Bensby et al. (2010b) in microlensed dwarf and subgiant stars of the Galactic bulge. In order to convert the data of Bensby et al. (2010b) to abundances by number, we used their solar abundances. The stellar ages were normalized to the age of the model ($t = 13.0$ Gyr).

Our model at $r = 3$ kpc successfully reproduces the O/Fe-Fe/H obtained by Bensby et al. (2010b), but the time-Fe/H relation is only partially reproduced. Our model explains all old-metal-poor stars and two young stars, but not the oldest metal-rich star in their sample (see the square at 12+log(Fe/H)$\sim$7.9) which behaves like a common bulge star, see Ballero et al. (2007). The youngest and more metal-rich stars would be disk stars that formed at $r < 3$ kpc.

Since Fe is produced by massive stars and binary systems of LIMS, to a first approximation Fe behaves like C, which is produced by MS and single LIMS, see for example Akerman et al. (2004), and the C/O-O/H discussion presented above can be used to explain the O/Fe-Fe/H and time-Fe/H panels of Figure 10.

Bensby et al. (2010a) have studied red giant stars in the inner Galactic disc and find that the abundance trends of the inner disc agree very well with those of the nearby thick disc, and also with those of the Galactic bulge. Based on the stellar results of the thick and thin disks of the solar vicinity, of the inner Galactic disc, and of the Galactic bulge (Bensby & Feltzing 2006; Bensby et al. 2010a,b), they suggest that the bulge and the disk have had similar chemical histories. Moreover, Alves-Brito et al. (2010) also suggest that the bulge and local thick disk stars formed over similar timescales with similar star formation rates and initial mass functions.

Cescutti et al. (2009) present a Galactic bulge model, computed by Ballero et al. (2007), in which, in order to reproduce the total stellar mass, the iron distribution function, and the α/Fe-Fe/H relations (all constraints obtained from giant stars) they assume: a formation time scale of $\sim$0.1 Gyr, as well as a star formation efficiency one order of magnitude higher and an IMF flatter for $m > 1\ M_\odot$ than those considered in our models. This model, with a SFR as long as 0.5 Gyr, cannot explain the ages of the youngest bulge dwarfs found by Bensby et al. (2010b).

Note that, if we focus only on the C/O-O/H and O/Fe-Fe/H relations determined in dwarf stars of the Galactic bulge, we cannot distinguish between a scenario with a very rapid infall, efficient star formation, and a high relative formation of massive stars –that by Cescutti et al. (2009)– and another scenario with an order of magnitude less rapid infall, an order of magnitude less efficient star formation, and a lower relative formation of massive stars – the one presented in this paper.

Nevertheless, if we focus on the age-Fe/H relation shown by bulge dwarf stars, our model, with an extended bulge formation time and therefore an extended star formation history, produces a better fit to the data than that by Cescutti et al. (2009).

In Figure 11 we show the iron distribution function predicted by the IWY model for $r = 3$ kpc in the Galactic disk from 0 to 7 Gyr. Since there are no good abundance determinations for the inner parts of the Galactic disk, we compare our model with the 104 stars that belong to the outermost field along the bulge minor axis at $b = -12$, see lower panel of Figure 14 by Zoccali et al. (2008). We have used 12+log(Fe/H)$_\odot$ = 7.50 to convert the [Fe/H] values of the Zoccali et al. (2008) sample to Fe/H abundances by number. From that figure, we can say that a non-negligible fraction of the stars in the direction of the bulge might belong to the inner disk. Moreover, about the bulge sample we note that: (i) for 12+log(Fe/H) < 7 the contamination of the thick disk is high, (ii) for $7 < 12 + \log(\mathrm{Fe/H}) < 8$ the contamination of the thin disk is lower and the true bulge stars dominate, and (iii) for 12+log(Fe/H) > 8 the contribution of the metal-rich stars of the thin disk is important.

Note that in Figure 11 we are using only the outermost 104 stars of the total of 800 stars located in the direction of the bulge, and the results of our model for $r = 3$ kpc. On the other hand Cescutti & Matteucci (2011) show that their bulge model (the same as Cescutti et al. 2009) follows the constraint provided by the 800 stars very well using a Salpeter IMF. The model by Cescutti and Matteucci predicts a smaller number of stars for [Fe/H] values higher than solar, probably indicating that the bulge sample has been contaminated by innermost disk stars.

From the previous discussion it follows that the Galactic bulge is a complex structure that should be studied further (e.g., Zoccali 2010).

7. CONCLUSIONS

We have constructed models with three different sets of yields that differ only on their Z dependence at solar metallicities for massive stars: HWY, IWY, and LWY. The HWY and the LWY have been used before by us, while in this paper we introduce the IWY, that are given by (HWY + LWY)/2. We find that the IWY Galactic chemical evolution models produce better fits to the observational data than either the HWY or the LWY models.

We present a Galactic chemical evolution model based on the IWY for the disk of the Galaxy that is able to fit: (a) the C/O vs O/H, C/Fe vs Fe/H, O/Fe vs Fe/H, and Fe/H vs t relations derived from halo and disk stars of different ages in the solar vicinity, (b) the O/H, C/H, and C/O abundance gradients (slopes and absolute values) derived from Galactic H II regions, (c) the He/H, C/H, O/H, Fe/H protosolar abundances, and (d) the He/H and O/H values of the Galactic H II region M17.

We find that in general about half of the freshly made helium is produced by massive stars and half by LIMS, and that a similar situation prevails for carbon, while most of the oxygen is produced by massive stars. The agreement of the He/O and C/O ratios between the model and the protosolar abundances implies that the Sun formed from a well mixed ISM.

We note that the agreement of our model with the protosolar abundances and the Sun-formation time supports the idea that the Sun originated at a Galactocentric distance similar to that of the solar vicinity.

We show that chemical evolution models for the Galactic disk are able to reproduce the observed ΔY and ΔO protosolar values and the ΔY and ΔO values derived for M17 based on H, He and O recombination lines, but not the M17 ΔY and ΔO values derived from T(4363/5007) and O collisionally excited lines under the assumption of $t^2 = 0.00$. This result provides a consistency check in favor of the presence of large temperature variations in H II regions and on the method based on the H, He, C and O recombination lines to derive abundances in H II regions.

We obtain that the IWY chemical evolution model of the Galactic disk for the present time, in the Galactocentric range $6 < r(\mathrm{kpc}) < 11$, produces a reasonable fit to the O/H vs C/O relationship derived from H II regions of nearby spiral galaxies. The yields predict an increase of the C/O ratio with O/H starting from 12+log(O/H)$\sim$8.4 which is observed in our Galaxy and in nearby galaxies. The O/H vs C/O relationship might imply that spiral galaxies have a similar IMF, no selective outflows, and probably a formation scenario similar to that of our galaxy.

We find a remarkable parallelism of the O/H gradients for M33, M101, and the Galaxy when they are plotted with respect to r/R_0 (R_0 is the galactic photometric radius to 25 mag per square second), suggesting some common mechanisms in the formation and evolution of spiral galaxies. The O/H ratio at a given r/R_0 differs by a constant among M33, M101 and the MW. The MW shows a 0.24 dex higher O/H ratio than the average of M33 and M101 at a given r/R_0.

We also find that the results for our model at $r = 3$ kpc can explain: (a) the C/O-O/H and O/Fe-Fe/H relations, and (b) partially the Fe/H-time relation and the Fe distribution function derived from stellar observations in the direction of the Galactic bulge. We find that stars belonging to the thin and thick discs make a significant contribution to these relations.

Future work to advance in this subject requires: (a) further studies of the Galactic bulge to be able to quantify the stellar contributions due to the inner disk and the true bulge; (b) to increase the H II regions r/R_0 coverage, mainly for the smaller galactocentric distances, with high accuracy C/H and O/H abundance determinations; (c) to increase the sample of spiral galaxies of different types with O/H gradients of high accuracy; and (d) to make specific models for each galaxy. All this is required to sort out possible differences in the galactic formation and evolution of other galaxies relative to that of the Galaxy.

We thank Jorge García-Rojas and César Esteban for useful discussions. We are also grateful to the anonymous referee for a careful reading of the manuscript and many excellent suggestions. This work was partly supported by the Conacyt grants 60354 and 129753.

REFERENCES

Alves-Brito, A., Meléndez, J., Asplund, M., Ramírez, I., & Yong, D. 2010, A&A, 513, 35

Akerman, C. J., Carigi, L., Nissen, P. E., Pettini, M., & Asplund, M. 2004, A&A, 414, 931

Anders, E., & Grevesse, N. 1989, Geochim. Cosmochim. Acta, 53, 197

Asplund, M., Grevesse, N., & Sauval, A. J. 2005, in Cosmic ASP Conf. Ser. 336, Abundances as Records of Stellar Evolution and Nucleosynthesis, ed. T. G. Barnes & F. N. Bash (San Francisco: ASP), 25

Asplund, M., Grevesse, N., Sauval, A. J., & Scott, P. 2009, ARA&A, 47, 481

Ballero, S. K., Matteucci, F., Origlia, L., & Rich, R. M. 2007, A&A, 467, 123

Bensby, T., Alves-Brito, A., Oey, M. S., Yong, D., & Meléndez, J. 2010a, A&A, 516, L13

Bensby, T., & Feltzing, S. 2006, MNRAS, 367, 1181

Bensby, T., et al. 2010b, A&A, 512, A41

Bromm, B., & Larson, R. V. 2004 ARA&A, 42, 79

Carigi, L. 1994, ApJ, 424, 181

__________. 1996, RevMexAA, 32, 179

__________. 2000, RevMexAA, 36, 171

__________. 2008, in The Metal-Rich Universe, ed. G. Israelian & G. Meynet (Cambridge: Cambridge Univ. Press), 415

Carigi, L., Colín, P., & Peimbert, M. 1999, ApJ, 514, 787

__________. 2006, ApJ, 644, 924

Carigi, L., Colín, P., Peimbert, M., & Sarmiento, A. 1995, ApJ, 445, 98

Carigi, L., & Hernández, X. 2008, MNRAS, 390, 582

Carigi, L., & Peimbert, M. 2008, RevMexAA, 44, 341 (Paper I)

Carigi, L., Peimbert, M., Esteban, C., & García-Rojas, J. 2005, ApJ, 623, 213

Cescutti, G., & Matteucci, F. 2011, A&A, 525, A126

Cescutti, G., Matteucci, F., Francois, P., & Chiappini, C. 2007, A&A, 462, 943

Cescutti, G., Matteucci, F., McWilliam, A., & Chiappini, C. 2009, A&A, 505, 605

Chiappini, C., Matteucci, F., & Gratton R. 1997, ApJ, 477, 765

Chiappini, C., Matteucci, F., & Meynet, G. 2003a, A&A, 410, 257

Chiappini, C., Romano, D., & Matteucci, F. 2003b, MNRAS, 339, 63

de Vaucouleurs, G., & Pence, W. D. 1978, AJ, 83, 1163

Esteban, C., Bresolin, F., Peimbert, M., García-Rojas, J., Peimbert, A., & Mesa-Delgado, A. 2009, ApJ, 700, 654

Esteban, C., García-Rojas, J., Peimbert, M., Peimbert, A., Ruiz, M. T., Rodríguez, M., & Carigi, L. 2005, ApJ, 618, L95

Esteban, C., Peimbert, M., Torres-Peimbert, S., & Escalante, V. 1998, MNRAS, 295, 401

Esteban, C., Peimbert, M., Torres-Peimbert, S., & Rodríguez, M. 2002, ApJ, 581, 241

Fenner, Y., & Gibson, B. K. 2003, PASA, 20, 189

Fierro, C. L., & Georgiev, L. 2008, RevMexAA, 44, 213

Fulbright, J. P., McWilliam, A., & Rich, R. M. 2007, ApJ, 661, 1152

García-Rojas, J., & Esteban, C. 2007, ApJ, 670, 457

Greggio, L., & Renzini, A. 1983, A&A, 118, 217

Grevesse, N., & Noels, A. 1993, in Origin and Evolution of the Elements, ed. N. Prantzos, E. Vangioni-Flam, & M. Cassé (Cambridge: Cambridge Univ. Press), 15

Grevesse, N., & Sauval, A. J. 1998, Space Sci. Rev., 85, 161

Hirschi, R. 2007, A&A, 461, 571

Hirschi, R., Meynet, G., & Maeder, A. 2005, A&A, 433, 1013

Kalberla, P. M. W., & Kerp, J. 2009, ARA&A, 47, 27

Karakas, A., & Lattanzio, J. C. 2007, PASA, 24, 103

Kewley, L. J., & Ellison, S. L. 2008, ApJ, 681, 1183

Kroupa, P., Tout, C. A., & Gilmore, G. 1993, MNRAS, 262, 545

Lodders, K. 2003, ApJ, 591, 1220

Lodders, K., Palme, H., & Gail, H.-P. 2009, in The Landolt-Börnstein, New Series, Vol. VI/4b, ed. J. E. Trümper (Berlin: Springer-Verlag), 560

Maeder, A. 1992, A&A, 264, 105

Magrini, L., Stanghellini, L., Corbelli, E., Galli, D., & Villaver, E. 2010, A&A, 512, 63

Marcon-Uchida, M. M., Matteucci, F., & Costa, R. D. D. 2010, A&A, 520, 35

Marigo, P., Bressan, A., & Chiosi, C. 1996, A&A, 313, 545

__________. 1998, A&A, 331, 564

Matteucci, F. 2001, Astrophysics and Space Science Library, Vol. 253, The Chemical Evolution of the Galaxy (Dordrecht: Kluwer), 293

Matteucci, F., & Chiappini, C. 1999, in Chemical Evolution from Zero to High Redshift, ed. J. R. Walsh & M. R. Rosa (Berlin: Springer-Verlag), 83

Matteucci, F., Franco, J., Francois, P., & Treyer, M. 1989, RevMexAA, 18, 145

Mattsson, L. 2010, A&A, 515, 68

Meléndez, J., et al. 2008, A&A, 484, L21

Meneses-Goytia, S., Carigi, L., & García-Rojas, J. 2011, Astrobiology, submitted

Mesa-Delgado, A., et al. 2009, MNRAS, 395, 855
Meynet, G., & Maeder, A. 2000, A&A, 361, 101
__________. 2002, A&A, 390, 561
Mollá, M., & Díaz, A. I. 2005, MNRAS, 358, 521
Navarro, J. F., Abadi, M. G., Venn, K. A., Freeman, K. C., & Anguiano, B. 2011, MNRAS, in press (arXiv:1009.0020)
Nordström, B, et al. 2004, A&A, 418, 989
Pagel, B. E. J. 2009, Nucleosynthesis and Chemical Evolution of Galaxies (Cambridge: Cambridge Univ. Press)
Peimbert, A., & Peimbert, M. 2010, ApJ, 724, 791
Peimbert, A., Peimbert, M., & Luridiana, V. 2002, ApJ, 565, 668
Peimbert, M. 1967, ApJ, 150, 825
Peimbert, M., Luridiana, V., & Peimbert, A. 2007, ApJ, 666, 636
Peimbert, M., & Peimbert, A. 2011, RevMexAA (SC), in press (arXiv:0912.3781)
Peimbert, M., Peimbert, A., Carigi, L., & Luridiana, V. 2010, in IAU Symp. 268, Light Elements in the Universe, ed. C. Charbonnel, M. Tosi, F. Primas, & C. Chiappini (Cambridge: Cambridge Univ. Press), 91
Portinari, L., Chiosi, C., & Bressan, A. 1998, A&A, 334, 505
Prantzos, N. 2008, EAS Publications Series, 32, 311 (arXiv:0709.0833)
Prantzos, N., Vangioni-Flam, E., & Chauveau, S. 1994, A&A, 285, 132
Przybilla, N., Nieva, M. F., & Butler, K. 2008, ApJ, 688, L103
Renda, A., Kawata, D., Fenner, Y., & Gibson, B. K. 2005, MNRAS, 356, 1071
Romano, D., Karakas, A. I., Tosi, M., & Matteucci, F. 2010, A&A, 522, 32
Roskar, R., Debattista, V. P., Stinson, G. S., Quinn, T. R., Tobias Kaufmann, T., & Wadsley, J. 2008, ApJ, 675, L65
Sánchez-Blázquez, P., Courty, S., Gibson, B. K., & Brook, C. B. 2009, MNRAS, 398, 591
Schaller, G., Schaerer, D., Meynet, G., & Maeder, A. 1992, A&AS, 96, 269
Simón-Díaz, S. 2010, A&A, 510, A22
Simón-Díaz, S., & Stasińska, G. 2011, A&A, 526, A48
Thielemann, F. K., Nomoto, K., & Hashimoto, M. 1993, in Origin and Evolution of the Elements, ed. N. Prantzos, et al.(Cambridge: Cambridge Univ. Press), 297
Tinsley, B. M. 1980, Fundam. Cosmic Phys., 5, 287
Vílchez, J. M., & Esteban, C. 1996, MNRAS, 280, 720
Vlajić, M., Bland-Hawthorn, J., & Freeman, K. C. 2011, ApJ, in press (arXiv:1101.0607)
Woosley, S. E., & Weaver, T. A. 1995, ApJS, 101, 181
Yin, J., Hou, L. K., Prantzos, T. A., Boissier, S., Chang, R. X., Shen, S. Y., & Zhangh, B. 2009 A&A, 505, 497
Zoccali, M. 2010, in IAU Symp. 265, Chemical Abundances in the Universe: Connecting First Stars to Planets, ed. K. Cunha, M. Spite, & B. Barbuy (Cambridge: Cambridge Univ. Press), 271
Zoccali, M., et al. 2008, A&A, 86, 177

Leticia Carigi and Manuel Peimbert: Instituto de Astronomía, Universidad Nacional Autónoma de México, Apdo. Postal 70-264, México 04510, D.F., Mexico (carigi, peimbert@astroscu.unam.mx).